Physica Medica 58 (2019) 121–130

Contents lists available at ScienceDirect

Physica Medica

journal homepage: www.elsevier.com/locate/ejmp

Original paper

Dependence of neutrons generated by ^{7}Li(p,n) reaction on Li thickness under free-air condition in accelerator-based boron neutron capture therapy system employing solid-state Li target

Satoshi Nakamura[a,b,*], Hiroshi Igaki[b,c], Hiroyuki Okamoto[a,b], Akihisa Wakita[c], Masashi Ito[d], Shoji Imamichi[b,e], Shie Nishioka[a,b], Kotaro Iijima[a], Hiroki Nakayama[a,f], Mihiro Takemori[a,f], Kazuma Kobayashi[c], Yoshihisa Abe[b,g], Kae Okuma[c], Kana Takahashi[c], Koji Inaba[c], Naoya Murakami[c], Yuko Nakayama[c], Teiji Nishio[h], Mitsuko Masutani[b,e,i], Jun Itami[a,b,c]

[a] Department of Medical Physics, National Cancer Center Hospital, Tsukiji 5-1-1, Chuo-ku, Tokyo 104-0045, Japan
[b] Division of Research and Development for Boron Neutron Capture Therapy, National Cancer Center Exploratory Oncology Research & Clinical Trial Center, Tsukiji 5-1-1, Chuo-ku, Tokyo 104-0045, Japan
[c] Department of Radiation Oncology, National Cancer Center Hospital, Tsukiji 5-1-1, Chuo-ku, Tokyo 104-0045, Japan
[d] Department of Radiology, National Center for Global Health and Medicine, Toyama 1-21-1, Shinjuku-ku, Tokyo 162-8655, Japan
[e] Division of Genetics, National Cancer Center Research Institute, Tsukiji 5-1-1, Chuo-ku, Tokyo 104-0045, Japan
[f] Department of Radiological Science, Graduate School of Human Health Sciences, Higashi-ogu 7-2-10, Arakawa-ku, Tokyo 116-8551, Japan
[g] Department of Radiological Technology, National Cancer Center Hospital, Tsukiji 5-1-1, Chuo-ku, Tokyo 104-0045, Japan
[h] Department of Medical Physics, Graduate School of Medicine, Tokyo Women's University, Kawada-cho 8-1, Shinjuku-ku, Tokyo 162-8666, Japan
[i] Department of Frontier Life Sciences, Nagasaki University Graduate School of Biomedical Sciences, Sakamoto 1-7-1, Nagasaki 852-8588, Japan

ARTICLE INFO

Keywords:
Boron neutron capture therapy (BNCT)
Accelerator-based BNCT
Dose related to generated neutrons in BNCT
Dependence of Li thickness

ABSTRACT

Purpose: An accelerator-based boron neutron capture therapy (BNCT) system with a solid-state Li target is reported to have degradation of the Li target. The degradation reduces the Li thickness, which may change spectra of the generated neutrons corresponding to the Li thickness. This study aims to examine the relationship between the Li thickness and the generated neutrons and to investigate the effects of the Li thickness on the absorbed dose in BNCT.

Method: The neutron energy spectra were calculated via Monte Carlo simulation for Li thicknesses ranging from 20 to 150 μm. Using the system, the saturated radioactivity of gold induced by reactions between ^{197}Au and the generated neutrons was evaluated with the simulation and the measurement, and those were compared. Additionally, for each Li thickness, the saturated radioactivity was compared with the number of generated neutrons. The absorbed doses delivered by ^{10}B(n,α)^{7}Li, ^{14}N(n,p)^{14}C, ^{1}H(n, g)^{2}H, and (n,n′) reactions in water were also calculated for each Li thickness.

Results: The measurement and simulation indicated a reduction in the number of neutrons due to the degradation of the Li target. However, the absorbed doses were comparable for each Li thickness when the requisite number of neutrons for BNCT was delivered. Additionally, the saturated radioactivity of ^{198}Au could be a surrogate for the number of neutrons even if the Li thickness was varied.

Conclusions: No notable effect to the absorbed dose was observed when required neutron fluence was delivered in the BNCT even if the degradation of the Li was observed.

1. Introduction

Clinical reports on boron neutron capture therapy (BNCT) have been published in many studies [1–10], and its biological effectiveness has been reported through *in vivo* and *in vitro* experiments [11–16]. In BNCT, adequate amount of compounds containing boron-10 are delivered to tumor cells, following which neutron irradiation is performed to kill the tumor cells using the ^{10}B(n, α)^{7}Li reaction. The particles generated in the reaction (i.e., ^{4}He and ^{7}Li) exhibit high linear energy transfer (LET). Thus, the relative biological effectiveness (RBE) of BNCT

* Corresponding author at: Tsukiji 5-1-1, Chuo-ku, Tokyo 104-0045, Japan.
E-mail address: satonaka@ncc.go.jp (S. Nakamura).

https://doi.org/10.1016/j.ejmp.2019.02.010
Received 19 November 2018; Received in revised form 22 January 2019; Accepted 12 February 2019
Available online 16 February 2019

is expected to be greater than that of conventional radiotherapies such as photons and electrons. For example, when sufficient ^{10}B compounds have been delivered to the cells, BNCT is expected to effectively kill cells that are resistant to conventional radiotherapy [13,15,17]. Boronophenylalanine (BPA) is the ^{10}B compound generally applied in BNCT [8]. Several clinical studies have been conducted using BPA at locations adjacent to nuclear reactors, such as the study performed at Kyoto University [1–4,10]. However, nuclear-reactor-based BNCT is not considered a standard treatment method, as it is difficult for hospitals to employ nuclear reactors as neutron sources [1–3,18,19].

Recent researches have indicated that accelerator-based neutron sources can be employed in BNCT [20–23]. Two reactions are generally utilized to generate neutrons in accelerator-based BNCT systems—$^{7}Li(p,n)^{7}Be$ and $^{9}Be(p,n)^{9}B$ [20–24]. Considering a constructed system, the maximum neutron energy of the first reaction is approximately 1 MeV (Q-value = − 1.644 MeV, i.e., the incident proton energy is approximately 2.5 MeV), whereas that of the other reaction is higher than a few MeV (Q-value = − 1.850 MeV, i.e., the incident proton energy is higher than 8 MeV) [20,24–29]. The advantage of the first reaction is that the lower neutron energy facilitates a relatively more compact BNCT system because the ideal neutron energy can be acquired without the need for a thick moderator. Therefore, the system is compact and can be easily installed in hospitals. The accelerator-based BNCT system evaluated in this study generates neutrons via the $^{7}Li(p,n)^{7}Be$ reaction. However, a disadvantage is that the melting point of Li is lower than that of Be [27,28]. Considering the above, the National Cancer Center Hospital (NCCH), Tokyo, Japan, is currently in the midst of installing an accelerator-based BNCT system with a solid-state Li target to evaluate the efficacy of BNCT in clinical oncology [24].

The accelerator-based BNCT system requires multiple reactions to acquire sufficient number of neutrons, which can result in high thermal loading [24,27,28]. A previous study has suggested that the Li target is expected to degrade due to ion impact, high operating temperature, and other factors resulting from proton bombardment [28]. The degradation may induce thinning of the Li target and reduction in the efficiency of neutron generation per unit of proton current [28,30]. In BNCT, the total absorbed dose is the sum of high-LET dose components and γ-ray [1]. The main γ-ray dose component is delivered from $^{1}H(n, g)^{2}H$ reaction [1]. The high-LET dose components are derived from the combined effects of the $^{10}B(n, \alpha)^{7}Li$, $^{14}N(n, p)^{14}C$, and (n, n') reactions [28,36]. Hence, there is a possibility that the degradation induces changes in these dose components because the generated neutron quality is changed. In the previous study on BNCT, Kobayashi *et al.* reported the doses delivered to a patient for various Li thicknesses when the incident proton energy was the near-threshold energy in the $^{7}Li(p, n)^{7}Be$ reaction [28]. It can be inferred from these reports that the Li thickness is important in an accelerator-based BNCT system with a solid-state Li target. However, although proton energy of more than 2.25 MeV is generally proposed in an accelerator-based BNCT system with a Li target because the $^{7}Li(p, n)^{7}Be$ reaction has a resonance cross-section at this energy, reports focused on Li thickness under this condition are not sufficient [20,23–26,31]. Therefore, this study aims to examine the relationship between the Li thickness and neutrons generated by the $^{7}Li(p,n)$ reaction and to investigate the effects of the absorbed dose components under free-air condition in BNCT when the incident proton energy is more than 2.25 MeV. Additionally, this study also investigates the effect of the Li thickness in BNCT in terms of the high-LET dose components related to the generated neutrons.

2. Methods

The experiments were performed using the accelerator-based BNCT system (manufactured by Cancer Intelligence Care Systems, Inc., Tokyo, Japan, (CICS)) at NCCH, which employs a solid-state Li target and supports a maximum proton current of 20 mA, although 12 mA is normally used in clinical conditions [24]. The Li target was produced by a thermal evaporation method under vacuum. The evaporation of Li occurred when a filament contained the Li was heated, and the Li was then attached to a target basement of the Li target. The nominal thickness of Li target was approximately 100 μm. Thus, the Li target could be available for the accelerator-based BNCT system. Protons with nominal mean energy of 2.5 MeV bombard on the Li target. Thus, the maximum energy of the generated neutrons after passing the Li target is approximately 8×10^{2}–9×10^{2} keV [20,24–29]. After the generated neutrons pass through the beam-shaping assemblies made of MgF_2 (Nippon Light Metal Co. Ltd., Tokyo, Japan, and CICS) [31], most of them are moderated to approximately under 10 keV.

In the accelerator-based BNCT system with a solid-state Li target, a reduction in the Li thickness may change the neutron energy spectrum and the number of generated neutrons. Thus, in BNCT, the absorbed doses induced by the reactions of $^{10}B(n, \alpha)^{7}Li$, $^{14}N(n, p)^{14}C$, $^{1}H(n, g)^{2}H$, and (n, n') may depend on the Li thickness. Hence, the effect of the Li thickness in BNCT was examined by simulations and experiments in this study. Additionally, this study examined whether the saturated radioactivity of gold, which was exposed to the neutrons generated for each Li thickness, was a surrogate for the total neutron flux reached at a patient.

To evaluate the neutron flux, the radioactivity induced in gold wires covered with/without cadmium was measured after being bombarded by certain number of neutrons generated by the accelerator-based BNCT system at the NCCH. The saturated radioactivity was calculated from the induced radioactivity [24]. The relationship between the generated neutrons and incident protons was then evaluated using the saturated radioactivity of the metals. Using a ratio of the gold with/without the cadmium, proportion of the thermal neutrons was evaluated. Additionally, to investigate the effects of the Li thickness in an accelerator-based BNCT system with a solid-state Li target, the generated neutrons for each Li thickness were examined using Monte Carlo simulation. The results of the simulations were compared with those of the measurements to validate the effect of Li thickness.

2.1. Radioactivity measurement

The induced radioactivity was measured using a high-purity germanium (HP-Ge) detector (ORTEC, GEM20P4-70, Oak Ridge, USA). In order to determine the radioactivity of the radionuclide, the detection efficiency of the HP-Ge detector for the measurement sample was first assessed via Monte Carlo simulations (GEANT4, ver. 10. 1) [32–35]. It should be noted that the detection efficiency of the HP-Ge detector was modeled via simulation in a previous study [35]. The detection efficiency contained the detector efficiency in this study. The measurement geometries for the induced radioactivity were reproduced in the simulation to obtain the detection efficiencies for each measurement. The events resulting from the reactions between the sample and the HP-Ge detector were counted using a multichannel analyzer (MCA 7600, SEIKO EG&G, Tokyo, Japan), and a Gamma-Studio system (SEIKO EG&G, Tokyo, Japan) was used to count the number of photoelectric events that occurred in the HP-Ge detector.

2.2. Measurement of the neutron flux per unit of proton current and evaluation of thermal neutrons and doses from $^{10}B(n,\alpha)^{7}Li$, $^{14}N(n, p)^{14}C$, and $^{1}H(n, g)^{2}H$ at a patient position

To elucidate the relationship between the number of generated neutrons and the number of irradiated protons, specific equations were used to evaluate the saturated radioactivity of the metal in units of Bq/mA [24]. The effects of fluctuations in the irradiated protons can be avoided by using the unit of Bq/mA. These equations are provided in equations (1)-(4) in the previous study [24]. In this study, the weight in equation (3) in the previous study was replaced with the number of atoms in the metal. It is well known that the saturated radioactivity is proportional to the neutron flux at a certain position in the neutron

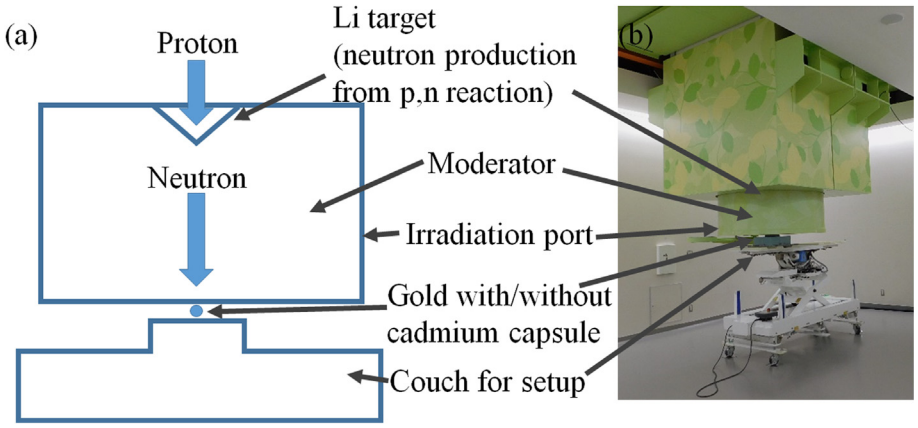

Fig. 1. (a) Schematic showing the neutron irradiation on the target metal, and (b): a photograph of the actual irradiation setup.

field. In this study, the saturated radioactivity was evaluated in place of the neutron flux because the saturated radioactivity is a reasonable surrogate of the neutron flux. Six Li targets were used to evaluate the reproducibility in this study.

The neutron flux was evaluated using a 99.5%-pure gold wire with 0.5-mm diameter and 8.0-mm length. The cadmium ratio was also evaluated to measure the proportion of thermal neutrons in the generated neutrons. The cadmium ratio was defined as the ratio of the saturated radioactivity of an un-encapsulated gold wire to that of a gold wire encapsulated with cadmium (0.5-mm thickness) [18,19]. In each evaluation of the saturated radioactivity, the number of protons delivered to the Li target was approximately 3.6×10^3 mC, and it was not exactly same. However, the cadmium ratio was calculated by each of the saturated radioactivity of an un-encapsulated gold wire and that of a gold wire encapsulated with cadmium. Cut-off energy of the cadmium capsule was approximately 0.55 eV since the thickness of cadmium capsule was 0.5 mm [37]. The measurement setup is shown in Fig. 1. In the measurement, the gold wires with and without the cadmium capsule were placed on the bottom surface of an irradiation port of the accelerator-based BNCT system at the center of the neutron field, and the neutrons were subsequently directed toward it. The gold wire encapsulated with the cadmium capsule was irradiated after the irradiation of the gold wire without the cadmium capsule, and the cadmium ratio was then evaluated. The reaction between the gold wire and the irradiated neutrons induced the formation of ^{198}Au, which subsequently emitted 412-keV gamma rays. The number of gamma rays was counted using the modeled HP-Ge detector to evaluate the neutron flux and the proportion of thermal neutrons in the neutron flux. In the dose components of BNCT, ^{10}B(n, α)^{7}Li, ^{14}N(n, p)^{14}C, and ^{1}H(n, g)^{2}H were induced by the reaction between the thermal neutrons and ^{10}B, ^{14}N, or ^{1}H in the human body [1]. Hence, an evaluation of the number of thermal neutrons is needed when these doses are calculated. Since the cadmium ratio represents a proportion of thermal neutrons in the neutron beam, the cadmium ratio could be surrogate for evaluation of these dose components when the requisite number of neutrons at the patient was delivered. In this study, the evaluation of these dose components was performed with evaluation of the cadmium ratio.

During irradiation, the number of irradiated protons was measured with an ammeter (NPCT-CF6, Bergoz Instrumentation, Saint-Genis-Pouilly, France) installed in the BNCT system, and the saturated radioactivity was evaluated for a certain amount of proton irradiation received at the Li target. A previous study suggested that the number of generated neutrons per unit of proton current decreases depending on the amount of proton irradiation delivered to the Li target due to the Li sputtering and the subsequent vaporization of the Li. Considering this, successive saturated radioactivity measurements were also performed [27–28]. The accumulated proton charges delivered in the intervals between the evaluations of the saturated radioactivity of the gold wire without the cadmium capsule was not above 86.4×10^3 mC, which is comparable to 2 h of irradiation with a proton current of 12.0 mA. On the other hand, that with the cadmium capsule was not above 30.2×10^4 mC. In this study, a unit of the accumulated proton charge is represented as "mA × h." Hence, proton charge of 86.4×10^3 mC is equivalent to 24.0 mA × h.

The cadmium ratios for each Li target were compared. Bartlett's test was used to examine whether the cadmium ratios were normally distributed. We used one-way ANOVA as a parametric test on these results. Additionally, if the cadmium ratio was not statistically significant for a Li target, we regarded all of the cadmium ratios as one group. Then, the cadmium ratios in the group were examined to check whether they were normally distributed by using the Shapiro–Wilk test. A *P*-value of less than 0.05 was considered statistically significant in this study.

2.3. Simulated neutron flux and dose from (n, n') reaction for each Li thickness

In this study, a Monte Carlo simulation (PHITS ver. 2.80) was used to quantify the effects of the Li thickness in the accelerator-based BNCT system [38]. The dose from the (n, n') reaction in the human body was evaluated to investigate the effect of each Li thickness on the absorbed dose from the high-LET dose component. The absorbed dose from the (n, n') reaction depended on the neutron energy although the absorbed doses from the ^{10}B(n, α)^{7}Li, ^{14}N(n, p)^{14}C, and ^{1}H(n, g)^{2}H reaction were affected by the number of thermal neutrons [1,36]. Therefore, the neutron energy spectrum delivered to a patient was evaluated in this study. The dose from the (n, n') reaction was defined as the neutron dose in this study. The neutron dose was calculated by multiplying the neutron flux at each energy, which was acquired with the simulation, by KERMA coefficients for water reported in ICRU 63 [36]. The neutron energy group structure comprised 56 groups in the energy range from 1.10×10^{-5} to 1.05 MeV in the simulation. The energy group structure was below the maximum generated neutron energy in the Li(p, n) reaction corresponding to that for the reported KERMA coefficient [36]. This process was separated into two stages. The simulation geometries of these processes are shown in Fig. 2. In the first stage, Monte Carlo simulation (PHITS) was used to evaluate the energy spectrum of the generated neutrons. Unfortunately, PHITS is not equipped with the cross-section files of the Li(p, n) reaction. Hence, the cross-section files in MCNP 6.1 were installed into PHITS, and the simulation was then performed [38,39]. The Li density was defined as 0.534 g/cm^3, and the Li thickness ranged from 20 to 150 μm in the simulation. The simulation geometry of the first stage is shown in Fig. 2(a). For each Li thickness, proton energy of 2.5 MeV was irradiated on the Li target, which had sufficient breadth to receive the proton beam. The neutrons across the bottom plane of the Li targets were evaluated in the simulation. The energy spectra of the generated neurons were compared for each Li

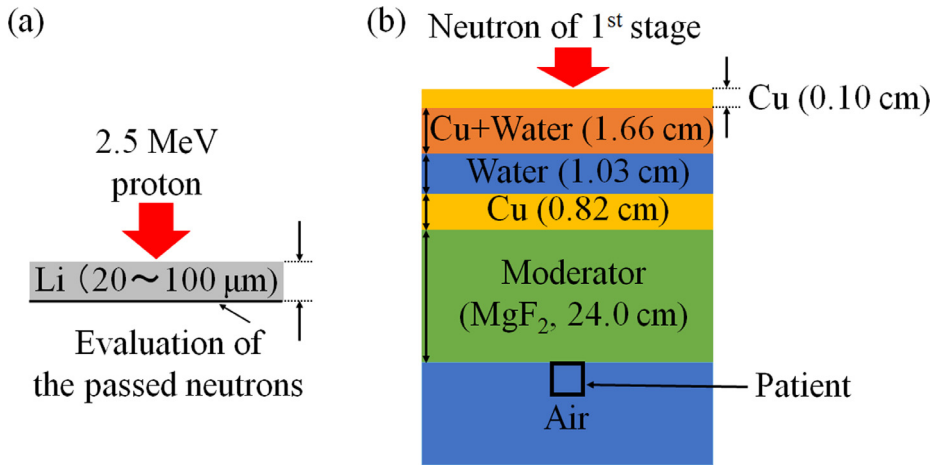

Fig. 2. (a): Schematic showing the simulation geometry of the reaction between Li target and protons, (b): Schematic showing the simulation geometry of the dose derived from the (n, n') reaction delivered to a patient.

thickness. Additionally, the proton path length for each residual proton energy value within the Li target was also calculated for each Li thickness. In this study, the residual proton energy in each Li thickness was divided into 25 energy groups, and the proton path length in each energy group was then evaluated. Interval of the energy group was uniform and its value was 0.1 MeV since the residual proton energy was between 0 and 2.5 MeV.

In the second stage, considering the application of BNCT in the treatment of patients, the accelerator-based BNCT system at NCCH was simply reconstructed on the simulation. The simulation geometry of the second stage is shown in Fig. 2(b). The simulation geometry consisted of the 1st copper support, mixture of cooling water and copper support, 2nd copper support, and the moderator made of MgF_2. The neutrons acquired for each Li thickness in the first stage were bombarded on the 1st copper support and passed on to the other layers. The patient, defined as a $1 \times 1 \times 1\ cm^3$ voxel, was placed at the center of the neutron irradiation in the second stage. The position of the patient corresponded to that in the measurement of saturated radioactivity in the previous subsection. The neutron energy spectrum at the patient location was calculated, followed by the calculation of the neutron dose delivered to the patient although material of the patient location was assumed as air in the simulation of neutron transport. Thus, the effects of each Li thickness on the neutron dose were evaluated. In order to compare the neutron flux between the measurement and the simulation, the saturated radioactivity of ^{198}Au was also calculated using the simulation result. For calculating the saturated radioactivity, the number of neutrons delivered to the patient was multiplied by the cross-sections of the capture reaction in ^{197}Au for each neutron energy. Additionally, for each Li thickness, the saturated radioactivity acquired with the simulation was compared with the total neutron flux, which was delivered to the patient, in the simulation to evaluate whether the value of the saturated radioactivity could be a surrogate for the total neutron flux. The Pearson's correlation coefficient was calculated to evaluate the correlation between the total neutron flux and the saturated radioactivity for each Li thickness. The total neutron flux per unit of proton and the saturated radioactivity per unit of proton at the patient end were evaluated to compare with the measurement results in the previous subsection. In the calculation, the lower cut-off energy was set to 11 eV because the $S(\alpha, \beta)$ library for layers such as the moderator was not available in the Monte Carlo simulation. The $S(\alpha, \beta)$ library is required to calculate the transport of low-energy neutrons accurately.

3. Results

3.1. Measurement of the neutron flux per unit of proton current and evaluation of thermal neutron and doses from $^{10}B(n,\alpha)^7Li$, $^{14}N(n, p)^{14}C$, and $^1H(n, g)^2H$ at a patient position

The measured neutron flux per unit of proton current and the cadmium ratio are shown in Fig. 3. In Fig. 3, the plots along to the horizontal axis were determined by the number of protons delivered to the Li target before each measurement of the saturated radioactivity with bare gold wire. As shown in Fig. 3(a), the neutron flux for each target reduced depending on the accumulated protons delivered on the Li

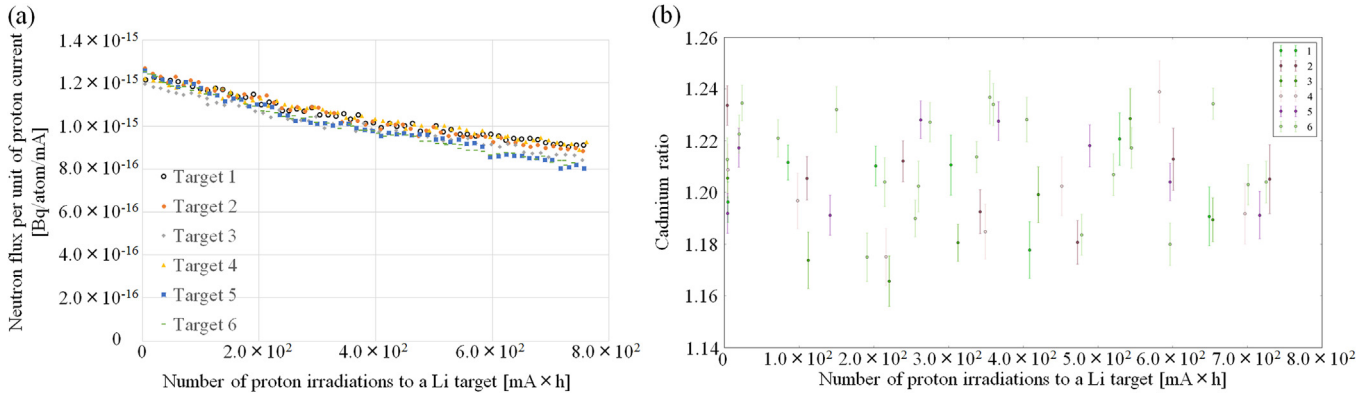

Fig. 3. (a) Neutron flux per unit of proton current and (b) cadmium ratio in each of the Li target along with the accumulated protons delivered to the Li target. The saturated radioactivity of ^{198}Au was used as a surrogate for the neutron flux. The ratio of the saturated radioactivity of ^{198}Au with and without the cadmium capsule was calculated as the cadmium ratio.

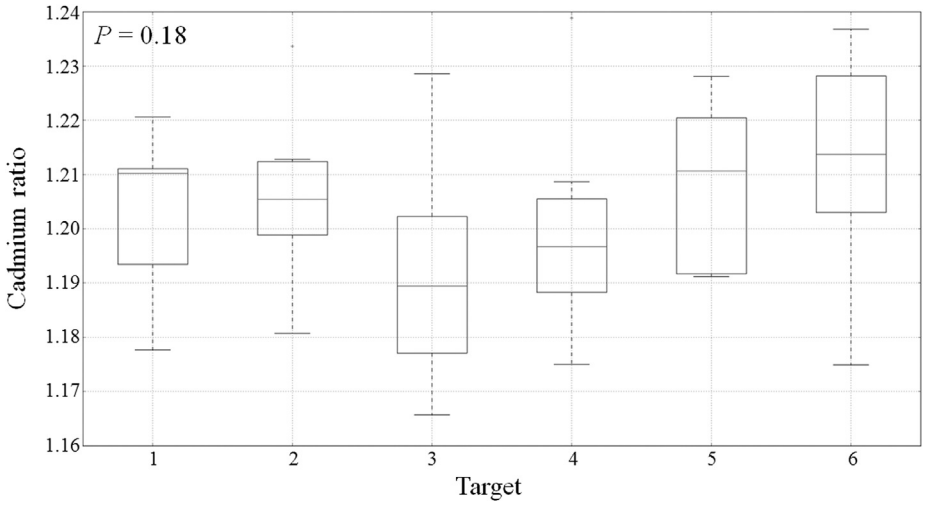

Fig. 4. Boxplot of the cadmium ratio in six Li targets.

target, following which the degradation of the Li target was observed. Additionally, the reduction in neutron flux did not change considerably with the accumulation of protons delivered to the Li target. The reduction in the neutron flux reached approximately 30% for the rise in the accumulated protons delivered to the Li target from 0 to 700 mA × h. The cadmium ratios were normally distributed ($P = 0.81$) among the six Li targets. According to the result of the one-way ANOVA test, the cadmium ratios of the six Li targets did not show a statistically significant difference ($P = 0.18$). The boxplot of the cadmium ratios in each Li target is shown in Fig. 4. The mean values and standard deviations (SD) of the cadmium ratios in the targets 1, 2, 3, 4, 5, and 6 were 1.20 ± 0.01, 1.21 ± 0.02, 1.19 ± 0.02, 1.20 ± 0.02, 1.21 ± 0.02, and 1.21 ± 0.01 (mean ± SD), respectively. We regarded all of the cadmium ratios as one group, and the Shapiro–Wilk test was applied to the group. The cadmium ratios in the group were normally distributed ($P = 0.21$). Additionally, the mean value and SD for all cadmium ratios was 1.21 ± 0.02. As shown in Fig. 3(b) and these results, the cadmium ratio was comparable at each accumulated value of protons delivered to the Li target. Hence, the proportion of the thermal neutron in the neutron flux was comparable for each amount of protons delivered to the Li target. Therefore, the doses from ^{10}B(n, α)^{7}Li, ^{14}N(n, p)^{14}C, and ^{1}H(n, g)^{2}H reaction delivered to the patient were comparable under free-air condition when the requisite number of neutrons for BNCT were delivered to the patient at each value of the accumulated proton irradiation on the Li target, as those doses were derived from the reaction between thermal neutron and ^{10}B, ^{14}N or ^{1}H in the patient.

3.2. Simulated neutron flux and dose from (n, n') reaction for each Li thickness

In order to verify the effects of the Li thickness in the accelerator-based BNCT system, the generated neutrons for each Li thickness was examined. Fig. 5(a) shows the mean proton path length at each value of the residual proton energy within the Li target. According to Fig. 5(a), the mean proton path lengths at residual energy between 2.2 and 2.3 MeV were comparable at the Li thickness of more than 50 μm, although it shortened at the Li thickness of less than 50 μm. The neutron energy spectrum for each Li thickness in the first stage is shown in Fig. 5(b). When the Li thickness was reduced, the number of generated neutrons was reduced at lower energy. Additionally, the number of generated neutrons at the neutron energy of 0.5 MeV was decreased for the Li thickness of less than 50 μm.

In the second stage, the neutron dose reaching the patient was calculated. For each Li thickness, the neutron energy spectrum and the neutron dose per unit of neutrons reaching the patient are shown in Figs. 6 and 7, respectively. The neutron doses per unit of the neutrons were comparable for each Li thickness. The difference between the neutron doses was within ± 4%. The saturated radioactivity per unit of proton and the number of neutrons per unit of proton delivered to the patient for each Li thickness are shown in Fig. 8. The saturated radioactivity per unit of protons was decreased by approximately 20% for the Li thickness between 50 and 100 μm. The total neutron flux and the saturated radioactivity depended on the Li thickness. The total neutron flux for each Li thickness was correlated with the corresponding saturated radioactivity, and the correlation coefficient between the two was 1.00. The trend of the reduction in saturated radioactivity for Li thickness of less than approximately 50 μm differed from that for the Li thickness of more than 50 μm. The reduction was greater in the case of Li thickness of less than approximately 50 μm.

4. Discussion

Previous reports have suggested that there are some challenges related to neutron generation in the accelerator-based BNCT system with a solid-state Li target [27,28]. The primary challenge is the reduction in the neutron flux per unit of proton current due to the degradation of the Li target [28]. Hence, this study focused on the degradation of the Li target, and its effects on the neutron generation was examined by using the accelerator-based BNCT system. The experiments and simulations in this study showed that the degradation of the Li target, such as the reduction in the Li thickness, could reduce the neutron flux. According to Fig. 8, when the Li thickness below 50 μm was decreased by the 10 μm in the simulation, the reduction of neutron flux expected approximately 15%. The decrease of Li thickness might be observed due to a thermal load to the Li target [28]. In each of the systems, cooling efficiency to remove the thermal load, which is induced by protons delivered to the Li target, are different. Hence, ratio of the reduction of neutron flux is not constant in every system. Therefore, in the system, this study suggested that the proton irradiations to the Li target of approximately 300–350 mAh expected to decrease the Li thickness of 10 μm in which the density was assumed as the theoretical density (Fig. 3(a)).

The Li target was produced by the thermal evaporation method in this study. According to the previous study, physical property of the Li target, such as a particle size, produced by the thermal evaporation method depends on several conditions of its method [40]. Although density of the Li target was assumed as 0.534 g/cc in the simulation, actual density of the Li target might be lower than its assumption. Unfortunately, the Li target under air condition is not utilized for the

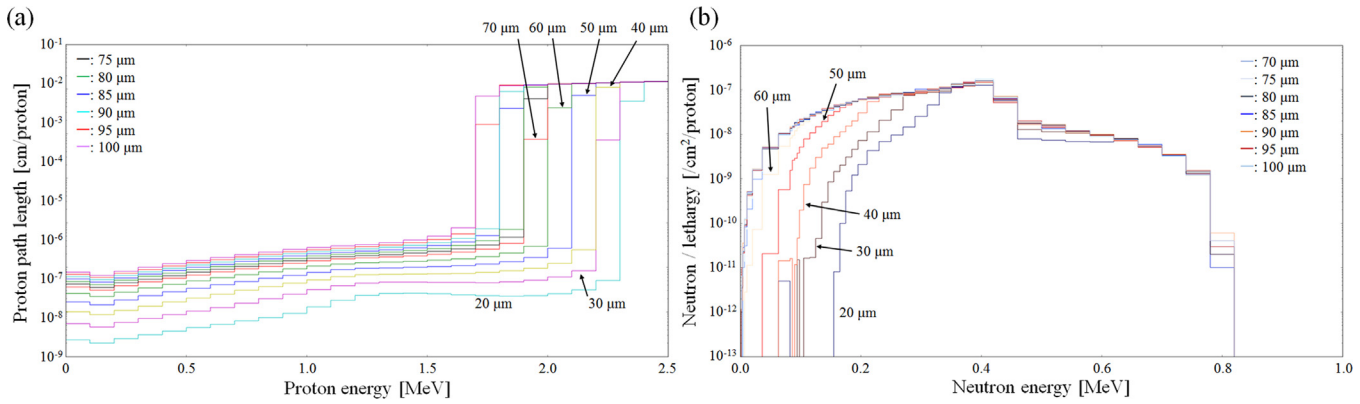

Fig. 5. (a) Evaluation of the proton path length at each value of the residual proton energy for various Li thicknesses. (b) Evaluation of the neutrons generated by Li (p,n) reaction for each Li thickness. These evaluation at the Li thickness of more than 100 μm is omitted because the proton path length related to the neutron generation is comparable at the Li thickness of more than 90 μm and the evaluation of the neutron generation is also consistent.

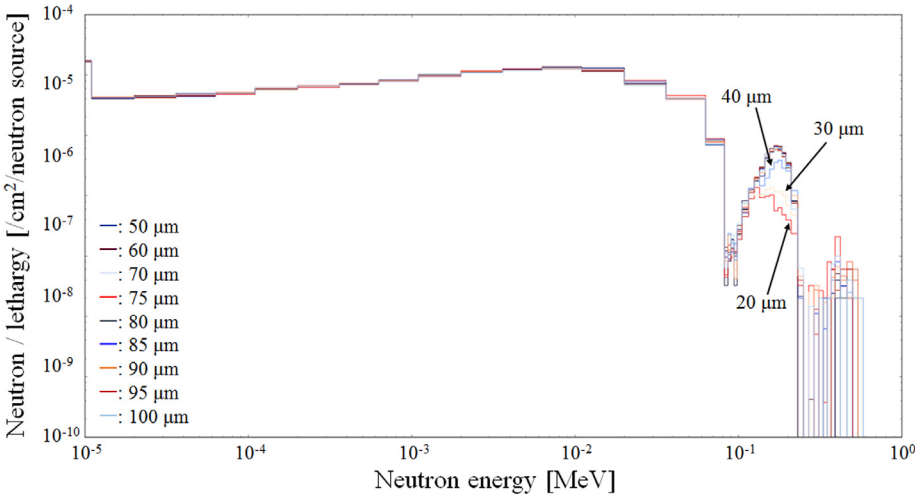

Fig. 6. Neutron energy spectrum at a patient surface for the Li thickness between 20 and 100 μm. The neutron energy spectrum at the Li thickness of more than 100 μm is omitted because difference of the neutron energy spectrum was not observed at the Li thickness of more than 50 μm.

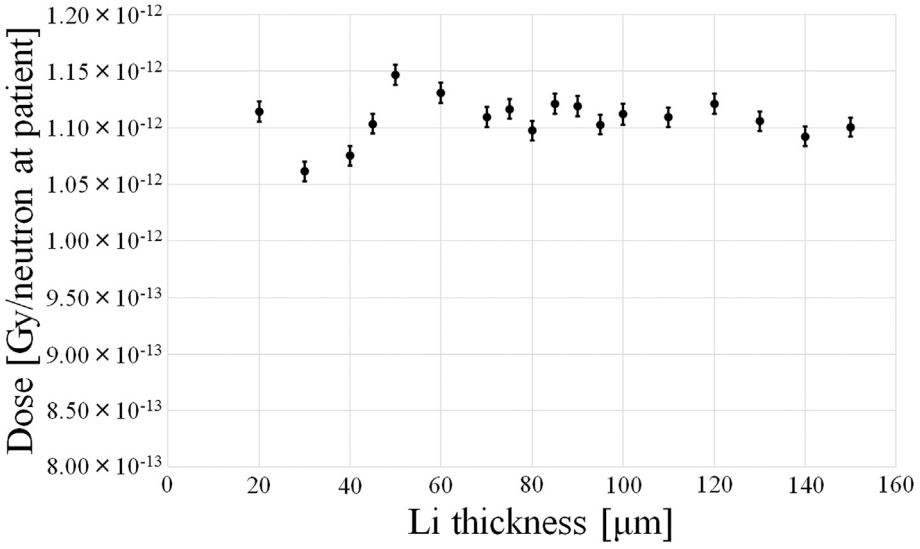

Fig. 7. Absorbed does derived from the (n, n') reaction per unit of neutrons reaching a patient for each Li thickness.

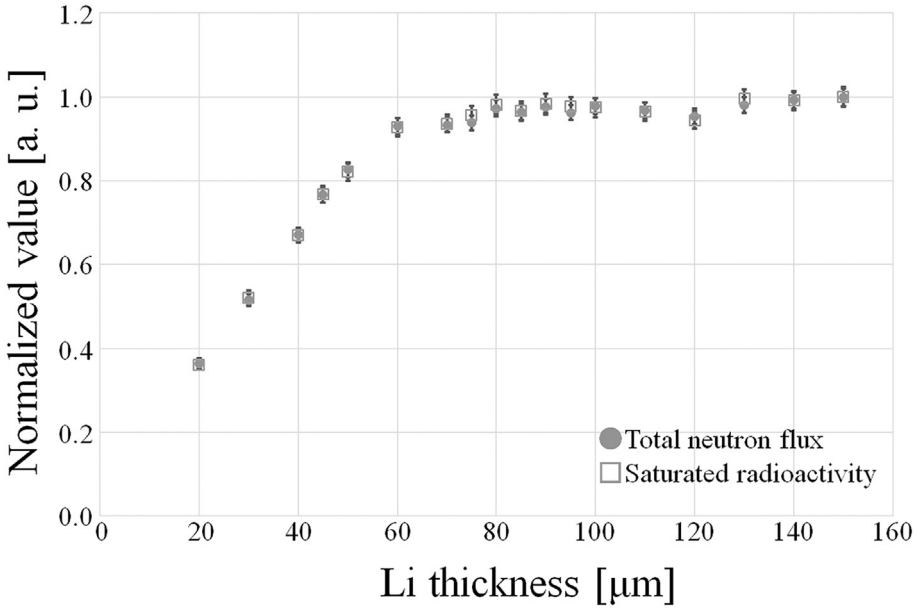

Fig. 8. Relationship between the number of neutrons and the saturated radioactivity at a patient surface for each Li thickness. These were evaluated based on per unit of protons delivered to the Li target.

accelerator-based BNCT system since the Li target easily reacts to water and nitrogen in the air. Thus, density measurement of the Li target with high accuracy could not be performed. However, according to Fig. 8, the reduction of neutron flux in Fig. 3(a) might suggest that the thickness of Li target with considering the actual density corresponded to the thickness of below 50 μm in the theoretical density of Li target (i.e., measurements of the saturated radioactivity of gold wire would be a surrogate for measurements of density and thickness of the Li target). Therefore, the degradation was observed since the actual density might be lower than 0.534 g/cc. Consideration of the density of Li target can be performed with multiplying the thickness of Li target by a ratio of the density. Therefore, it may be important for designing an accelerator-based BNCT system with the Li target that the density of Li target was considered. Additionally, the effects of Li thickness to the low energy neutrons might be observed in the measurements of this study. According to Fig. 3(b), the cadmium ratio was comparable at each number of protons delivered to the Li target although the thickness of Li target might be reduced. The cadmium ratio plays an important role for evaluations of thermal neutron. Cut-off energy of the cadmium capsule was approximately 1 eV. Since the cut-off energies of cadmium capsule and the lowest energy in the simulation were approximately comparable, the measurement result of cadmium ratio might ensure a result of lower than the 11 eV in the simulation. In these reasons, the low energy neutrons did not depend on the Li thickness in case of the accelerator-based BNCT system. Therefore, this study investigated that absorbed doses from thermal neutron reaction was comparable in each Li thickness.

This study analyzed whether the measurement of the saturated radioactivity of ^{198}Au induced by the neutron bombarded on gold for each Li thickness could be a surrogate for the measurement of the total neutron flux for each Li thickness. Fig. 8 shows that the saturated radioactivity of ^{198}Au for each Li thickness is correlated with the corresponding total neutron flux. Therefore, the saturated radioactivity of ^{198}Au can be a surrogate of the total neutron flux for each Li thickness in an accelerator-based BNCT system employing a Li target.

This study investigated that the range of an incident proton energy of 2.5 MeV in the Li target was approximately 90 μm (Fig. 5). This result was consistent to the previous study [29]. The previous study also suggested that the Li thickness of approximately 35–40 μm is required to decelerate 2.5-MeV protons to the resonance energy at 2.25 MeV in the ^{7}Li(p,n) reaction [29]. According to Fig. 5(a), the required thickness for decelerating the proton energy to 2.25 MeV was between 30 and 40 μm, and its result was also consistent to the previous study [29]. However, it did not mean that the required thickness for decelerating the proton energy to 2.25 MeV stably acquired the neutron generations with its energy. If the Li thickness between 35 and 40 μm stably acquired the neutron generation with the proton energy of 2.25 MeV, a trend of the number of neutrons at the patient was not same in the Li thickness of 50 μm (i.e., the treand was same in the Li thickness of equal to or less than 40 μm while it was not same in the Li thickness of 50 μm). According to Fig. 8, the trend of the number of generated neutrons with the Li thickness of equal to or less than 50 μm was same. Therefore, we thought that evaluations of the sufficient proton path length in each residual proton energy was suitable for the evaluation of Li thickness dependence rather than evaluations of proton range in the Li target.

According to Fig. 5, the number of generated neutrons with an energy of approximately 0.5 MeV was reduced in the case of Li thickness of less than 50 μm. These generated neutrons were induced by the reaction between Li and proton with an energy of 2.25 MeV because the *Q*-value of the reaction was −1.850 MeV. Therefore, the number of generated neutrons was considerably reduced for Li thickness of less than approximately 50 μm because the proton path length was not sufficient to decelerate the residual proton energy within the Li target to the resonance energy of the ^{7}Li(p, n)^{7}Be reaction.

In BNCT, the absorbed dose related to the generated neutrons is derived from the ^{10}B(n, α)^{7}Li, ^{14}N(n, p)^{14}C, ^{1}H(n, g)^{2}H, and (n, n') reactions in the composition substances of the human body [1]. The doses from the ^{10}B(n, α)^{7}Li, ^{14}N(n, p)^{14}C, and ^{1}H(n, g)^{2}H reactions are delivered to a patient due to the thermal neutron fluence. Hence, the number of thermal neutrons is important for BNCT. Nevertheless, the low-energy neutrons were ignored in the simulation. However, the thermal neutrons were measured using the cadmium ratio in this study. According to Fig. 3(b) and 4, the values of the cadmium ratio were constant for 0–700 mA × h of protons delivered to the Li target. These results suggested that the proportion of thermal neutrons in the generated neutrons reaching the patient was consistent for each accumulated value of protons delivered to the Li target. Hence, the proportions of thermal neutrons were also comparable for each Li thickness in the accelerator-based BNCT system. Thus, the saturated radioactivity of ^{198}Au and the total neutron flux for each Li thickness showed the same

trends in Fig. 8 even when low-energy neutrons were considered in the calculation. Additionally, this result also suggested that the doses from $^{10}B(n, \alpha)^{7}Li$, $^{14}N(n, p)^{14}C$, and $^{1}H(n, g)^{2}H$ were comparable under free-air condition when the requisite number of neutrons were irradiated, even if the Li target was degraded. On the other hand, the neutron dose derived from the (n, n') reaction depended on the neutron energy spectrum at a certain position. However, according to Fig. 7, the neutron doses per unit of the neutrons reaching the patient were comparable for Li thickness of more than 20 μm because the neutron energy spectrum for each Li thickness did not have considerable difference at the patient location. Hence, these results indicated that the absorbed doses related to the generated neutrons were comparable when the requisite number of neutrons for BNCT was delivered to the patient, even if the Li target was degraded. Therefore, it may be necessary to develop a technique for delivering the required number of neutrons in the accelerator-based BNCT system to overcome the effects of degradation of the Li target.

Additionally, in the accelerator-based BNCT system, gamma ray doses associated with an incident protons to the Li target have to be considered. Those gamma rays are induced by an inelastic proton scattering reaction of $^{7}Li(p,p'\gamma)$ in the Li target and by a proton capture reaction of $^{7}Li(p,\gamma)$ when an incident proton energy is equaled to or less than 2.5 MeV. The gamma ray energy from the inelastic proton scattering reaction is 478 keV [26,41]. According to previous study [26], a ratio of the gamma ray yields to the neutron yields was 0.419–25.10 in case of the proton energy ranged from 1.89 to 2.50 MeV. In the accelerator-based BNCT system with an incident proton energy of 2.5 MeV, a certain thickness of moderator is required to acquire the suitable neutron energy for BNCT [26]. In this system, the moderator made of MgF_2 is equipped, and its thickness is 24 cm. Hence, the gamma ray is attenuated by the moderator. According to previous study, a mass attenuation coefficient of water with a gamma ray energy of 500 keV is 9.667×10^{-2} cm^2/g [42]. Hence, the gamma ray associated with the inelastic proton scattering reaction is less than 1×10^{-5}% even if a density of the moderator is applied to the mass attenuation coefficient of water (i.e., A mass attenuation coefficient of MgF_2 would be higher than that of water). Additionally, according to previous study, the gamma ray dose associated with the protons delivered to the Li target was less than half of that associated with the neutron capture reaction in human nevertheless the moderator did not equip [28]. Therefore, these reasons investigated that the gamma ray associated with the inelastic proton scattering reaction could be ignored in terms of effect of the Li thickness to the absorbed dose in the accelerator-based BNCT system. Additionally, in the gamma rays derived from the reaction of $^{7}Li(p,\gamma)$, according to the previous study, this reaction can be neglected because the gamma ray yields from its reaction is at least three orders of magnitude lower than that of $^{7}Li(p,p'\gamma)$ reaction [26].

The limitations of this study are as follows. The simulation geometry was not reconstructed in detail; the cross section of the $^{7}Li(p,n)$ reaction on MCNP 6 might not be precise; the library of $S(\alpha, \beta)$ was not applied to the simulation; the doses related to the generated neutrons were evaluated under free-air condition; and protons with incident energy of 2.5 MeV were considered. The simulation geometry may affect the neutron energy. Actually, Fig. 3(a) indicates that the trend of the measured saturated radioactivity did not change considerably for 0–700 mA × h of protons delivered to the Li target whereas the corresponding reduction in saturated radioactivity was approximately 30%. According to Fig. 8, if the reduction in saturated radioactivity is 30%, the trend of the saturated radioactivity changes considerably (i.e., the Li thickness decreases from more than 100 μm to 40 μm). In the simulation, the trend changes at the Li thickness of approximately 50 μm. This discrepancy may be caused because the actual geometry of the accelerator-based BNCT system has more complex beam-shaping assembly, such as the inclusion of a reflector for generated neutrons [43]. However, according to Fig. 7, the effects of the Li thickness on the absorbed doses in BNCT might be negligible even if the neutron energy spectrum changes slightly. This is because the energy spectrum of the generated neutrons is determined by the proton energy, the proton path length in the Li target at each residual proton energy value, and the relevant aspects of the Li(p, n) reaction, such as the *Q*-value. Actually, although the energy spectrum changed slightly for each Li thickness (Fig. 5), the neutron dose was comparable. Hence, the neutron dose per unit of neutron might be constant for proton irradiation between 0 and 700 mA × h delivered to the Li target. Therefore, in an accelerator-based BNCT system employing a Li target, the effect of each Li thickness on the absorbed doses corresponding to the generated neutrons might be too low to affect the BNCT. Lee and Zhou reported the cross section at a proton energy of under 2.5 MeV [25]. In the proton energy region, the cross section in MCNP6 was different from that reported by Lee and Zhou. However, a shape of the cross section along to incident proton energy of equal to or under 2.5 MeV was comparable. Therefore, although the number of generated neutrons might be overestimated in this study, the neutron dose per unit of neutrons reaching a patient in each Li thickness might be comparable since the shape of cross-section was comparable. Additionally, a shape of the neutron energy spectrum might be also comparable although the number of generated neutrons at each energy was different. The measurement results of Fig. 3(b) and 4 might compensate lacks of the simulation results of low energy neutrons although the library of $S(\alpha, \beta)$ was not applied to the simulation. The cadmium ratio plays an important role for evaluation of the low energy neutrons, such as thermal neutrons. Therefore, the results of Fig. 3(b) and 4 indicated that the low energy neutrons were evaluated in this study although the simulation did not contain those evaluation. Additionally, according to Fig. 6, the effects of Li thickness to the neutrons around 11 eV is not observed. Thus, the library of $S(\alpha, \beta)$ might not significantly affect the result of this study. In this study, evaluations of the absorbed doses were performed under free-air condition. The KERMA coefficient is generally higher in a neutron with higher energy, and the neutron dose with higher energy neutrons is higher than that with lower energy neutrons [36]. The neutron energy within a phantom is generally lower than that under free-air because of neutron moderation within the phantom. Therefore, the dose derived from the (n, n') reaction under free-air condition is more sensitive than that within the phantom. Hence, the effect of each Li thickness was evaluated in this study under the free-air condition. According to Fig. 7, the neutron doses per unit of the neutrons reaching the patient was comparable under free-air. Additionally, Fig. 4 showed that the proportion of thermal neutron in the neutron flux delivered to the patient was consistent even when the Li thickness was reduced due to degradation. Therefore, the absorbed doses derived from the $^{10}B(n, \alpha)^{7}Li$, $^{14}N(n, p)^{14}C$, $^{1}H(n, g)^{2}H$, and (n, n') reactions in the human body were comparable when the requisite number of neutrons for BNCT were delivered to the patient. However, the application of a phantom in the evaluation may require increasing the thermal neutrons due to neutron moderation within the phantom. In BNCT, the absorbed doses derived from the $^{10}B(n, \alpha)^{7}Li$, $^{14}N(n, p)^{14}C$, and $^{1}H(n, g)^{2}H$ reactions are induced by the thermal neutrons. Actually, the previous study indicated that the dose derived from the $^{10}B(n, \alpha)^{7}Li$ reaction reaches approximately 50% of the total dose in a normal tissue after considering the RBE in each dose component. Hence, in future studies, it may be necessary to evaluate the effects of each Li thickness on these doses using a phantom. The proton energy of 2.5 MeV acquires sufficient neutron flux for BNCT while keeping the generated neutron energy low in the accelerator-based BNCT system employing the Li target. Therefore, the proton energy of approximately 2.5 MeV is considered in the construction of the accelerator-based BNCT system. On the other hand, when the proton energy of more than 2.5 MeV is adopted in an accelerator-based BNCT system with a Li target, the effects of each Li thickness may be observed because of the $^{7}Li(p, n)^{7}Be^{*}$ reaction [29]. According to Figs. 5(a) and 6, the effect of the Li thickness on the generated neutron with low energy was negligible in the accelerator-based BNCT system because the generated neutrons were moderated by

the moderator and the generated neutrons at low energy did not reach the patient. On the other hand, its effect was observed on the generated neutrons with high energy although the absorbed doses per unit of neutrons were not affected in the BNCT. These effects need to be considered when the ^{7}Li(p, n)^{7}Be* reaction is utilized.

5. Conclusion

This study focused on the effects of Li thickness in the accelerator-based BNCT system with a solid-state Li target in terms of the degradation of the Li target. This study observed that the reduction in the neutron flux per unit of protons delivered to the Li target is due to the degradation. The degradation induced a reduction in the Li thickness in the accelerator-based BNCT system with a Li target. For each Li thickness, it was found that the neutron doses per neutron derived from the (n, n') reaction, reaching the patient, were comparable in the accelerator-based BNCT system because the neutron energy spectrum at the patient changed negligibly in the BNCT. Additionally, the doses per neutron derived from the ^{10}B(n, α)^{7}Li, ^{14}N(n, p)^{14}C, and ^{1}H(n, g)^{2}H reactions, reaching the patient, were consistent for each Li thickness. This was because the proportion of thermal neutrons in the neutron flux at the patient was constant although the Li target was degraded. Therefore, the effect of each Li thickness on the doses in terms of the generated neutrons is comparable when the requisite number of neutrons for BNCT is delivered. It was also found that measurements of the saturated radioactivity of ^{198}Au could be a reasonable surrogate for the measurement of the number of generated neutrons in an accelerator-based BNCT system. Using the above knowledge, BNCT can be performed as a suitable radiation therapy with an accelerator-based BNCT system employing a solid-state Li target although the system has some difficulties associated with neutron generation.

Conflict of interest Notification

Declarations of interest: none

Acknowledgments

This work was supported by a JSPS Grant-in-Aid for Young Scientists (B) (Grant Number 26860410), partially supported by a JSPS Grant-in-Aid for Scientific Research (B) (Grant Number 15H04912), by a JSPS Grant-in-Aid for Scientific Research (C) (Grant Number 16K10410), by the Medical Research and Development Programs Focused on Technology Transfer: Development of Advanced Measurement and Analysis Systems (SENTAN) from the Japan Agency for Medical Research and Development, AMED (17hm0102046s0505), and by the National Cancer Center Research and Development Fund (29-A-8), (26-A-18), and (23-A-46). We thank Dr. Hitoshi Nakagama, Dr. Yasuaki Arai, Dr. Tomomitsu Hotta, Dr. Takamasa Kayama, and the other staff members at the National Cancer Center for supporting our project for the development of an accelerator-based BNCT system.

References

[1] Kato I, Ono K, Sakurai Y, Ohmae M, Maruhashi A, Imahori Y, et al. Effectiveness of BNCT for recurrent head and neck malignancies. Appl. Radiat. Isot. 2004;61(5):1069–73.
[2] Nakai K, Yamamoto T, Aiyama H, Takada T, Yoshida F, Kageji T, et al. Boron neutron capture therapy combined with fractionated photon irradiation for glioblastoma: a recursive partitioning analysis of BNCT patients. Appl. Radiat. Isot. 2011;69(12):1790–2.
[3] Aihara T, Morita N, Kamitani N, Kumada H, Ono K, Hiratsuka J, et al. BNCT for advanced or recurrent head and neck cancer. Appl. Radiat. Isot. 2014;88:12–5.
[4] Futamura G, Kawabata S, Siba H, Kuroiwa T, Suzuki M, Kondo N, et al. A case of radiation-induced osteosarcoma treated effectively by boron neutron capture therapy. Radiat. Oncol. 2014;9:237.
[5] Sweet WH, Javid M. The possible use of slow neutrons plus boron10 in therapy of intracranial tumors. Trans. Am. Neurol. Assoc. 1951;56:60–3.
[6] Farr LE, Sweet WH, Robertson JS, Foster CG, Locksley HB, Sutherland DL, et al. Neutron capture therapy with boron in the treatment of glioblastoma multiforme. Am. J. Roentgenol. Radium Ther. Nucl. Med. 1954;71(2):279–93.
[7] Hatanaka H, Sano K. A revised boron-neutron capture therapy for malignant brain tumors. I. Experience on terminally ill patients after Co-60 radiotherapy. Z. Neurol. 1973;204(4):309–32.
[8] Mishima Y, Honda C, Ichihashi M, Obara H, Hiratsuka J, Fukuda H, et al. Treatment of malignant melanoma by single thermal neutron capture therapy with melanoma-seeking ^{10}B-compound. Lancet 1989;2(8659):388–9.
[9] Finkel GC, Poletti CE, Fairchild RG, Slatkin DN, Sweet WH. Distribution of ^{10}B after infusion of Na2^{10}B12H11SH into a patient with malignant astrocytoma: implications for boron neutron capture therapy. Neurosurgery 1989;24(1):6–11.
[10] Wang LW, Chen YW, Ho CY, Hsueh Liu YW, Chou FI, Liu YH, et al. Fractionated boron neutron capture therapy in locally recurrent head and neck cancer: a prospective phase I/II trial. Int. J. Radiat. Oncol. Biol. Phys. 2016;95(1):396–403.
[11] Saris SC, Solares GR, Wazer DE, Cano G, Kerley SE, Joyce MA, et al. Boron neutron capture therapy for murine malignant gliomas. Cancer Res. 1992;52(17):4672–7.
[12] Protti N, Manera S, Prata M, Alloni D, Ballarini F, di Tigoliole AB, et al. Gamma residual radioactivity measurements on rats and mice irradiated in the thermal column of a TRIGA Mark II reactor for BNCT. Health Phys. 2014;107(6):534–41.
[13] Masunaga S, Sakurai Y, Tanaka H, Tano K, Suzuki M, Kondo N, et al. The dependency of compound biological effectiveness factors on the type and the concentration of administered neutron capture agents in boron neutron capture therapy. SpringerPlus 2014;3:128.
[14] Watanabe T, Tanaka H, Fukutani S, Suzuki M, Hiraoka M, Ono K. L-phenylalanine preloading reduces the ^{10}B(n, α)^{7}Li dose to the normal brain by inhibiting the uptake of boronophenylalanine in boron neutron capture therapy for brain tumours. Cancer Lett. 2016;370(1):27–32.
[15] Hirota Y, Masunaga S, Kondo N, Kawabata S, Hirakawa H, Yajima H, et al. High linear-energy-transfer radiation can overcome radioresistance of glioma stem-like cells to low linear-energy-transfer radiation. J. Radiat. Res. 2013;55(1):75–83.
[16] Sun T, Zhang Z, Li B, Chen G, Xie X, Wei Y, et al. Boron neutron capture therapy induces cell cycle arrest and cell apoptosis of glioma stem/progenitor cells in vitro. Radiat. Oncol. 2013;8(1):195.
[17] Nakamura S, Murakami N, Inaba K, Wakita A, Kobayashi K, Takahashi K, et al. After low and high dose-rate interstitial brachytherapy followed by IMRT radiotherapy for intermediate and high risk prostate cancer. BMC Cancer 2016;16:296.
[18] Sakurai Y, Kobayashi T. The medical-irradiation characteristics for neutron capture therapy at the Heavy Water Neutron Irradiation Facility of Kyoto University Research Reactor. Med. Phys. 2002;29(10):2328–37.
[19] Sakurai Y, Kobayashi T. Spectrum evaluation at the filter-modified neutron irradiation field for neutron capture therapy in Kyoto University Research Reactor. Nucl. Instrum. Methods Phys. Res. A 2004;531(3):585–95.
[20] Kamada S, Takada M, Suda M, Hamano T, Imaeki H, Hoshi M, et al. Development of target system for intense neutron source of p-Li reaction. Appl. Radiat. Isot. 2014;88:195–7.
[21] Kumada H, Matsumura A, Sakurai H, Sakae T, Yoshioka M, Kobayashi H, et al. Project for the development of the linac based NCT facility in University of Tsukuba. Appl. Radiat. Isot. 2014;88:211–5.
[22] Tanaka H, Sakurai Y, Suzuki M, Masunaga S, Mitsumoto T, Fujita K, et al. Experimental verification of beam characteristics for cyclotron-based epithermal neutron source (C-BENS). Appl. Radiat. Isot. 2011;69(12):1642–5.
[23] Randers-Pehrson G, Brenner DJ. A practical target system for accelerator-based BNCT which may effectively double the dose rate. Med. Phys. 1998;25(6):894–6.
[24] Nakamura S, Imamichi S, Masumoto K, Ito M, Wakita A, Okamoto H, et al. Evaluation of radioactivity in the bodies of mice induced by neutron exposure from an epi-thermal neutron source of an accelerator-based boron neutron capture therapy system. Proc. Jpn. Acad. Ser. B Phys. Biol. Sci. 2017;93(10):821–31.
[25] Lee CL, Zhou XL. Thick target neutron yields for the ^{7}Li(p, n)^{7}Be reaction near threshold. Nucl. Instrum. Methods Phys. Res. B. 1999;152:1–11.
[26] Lee CL, Zhou XL, Kudchadker RJ, Harmon F, Harker YD. A Monte Carlo dosimetry-based evaluation of the ^{7}Li(*p*, n)^{7}Be reaction near threshold for accelerator boron neutron capture therapy. Med. Phys. 2000;27(1):192–202.
[27] Tanaka K, Yokobori H, Endo S, Kobayashi T, Bengua G, Saruyama I, et al. Characteristics of proton beam scanning dependent on Li target thickness from the viewpoint of heat removal and material strength for accelerator-based BNCT. Appl. Radiat. Isot. 2009;67(2):259–65.
[28] Kobayashi T, Bengua G, Tanaka K, Nakagawa Y. Variations in lithium target thickness and proton energy stability for the near-threshold ^{7}Li(p, n)^{7}Be accelerator-based BNCT. Phys. Med. Biol. 2007;52(3):645–58.
[29] Liskien H, Paulsen A. Neutron production cross sections and energies for the reactions ^{7}Li(*p*, n)^{7}Be and 7Li(p, n)^{7}B^{e*} *At.* Data Nucl. Data Tables 1975;15(1):57–84.
[30] Nkciles RJ. A high pressure gas target for cyclotrons. Nucl. Instrum. Meth. 1980;177:593–4.
[31] Inoue R, Hiraga F, Kiyanagi Y. Optimum design of a moderator system based on dose calculation for an accelerator driven Boron Neutron Capture Therapy. Appl. Radiat. Isot. 2014;88:225–8.
[32] Agostinelli S, Allison J, Amako K, Apostolakis J, Araujo H, Arce P, et al. GEANT4—a simulation toolkit. Nucl. Instrum. Methods Phys. Res. A 2003;506(3):250–303.
[33] Hurtado S, García-León M, García-Tenorio R. Monte Carlo simulation of the response of a germanium detector for low-level spectrometry measurements using GEANT4. Appl. Radiat. Isot. 2004;61:139–43.
[34] Ewa IO, Bodizs D, Czifrus S, Molnar Z. Monte Carlo determination of full energy peak efficiency for a HPGe detector. Appl. Radiat. Isot. 2001;55:103–8.
[35] Nakamura S, Wakita A, Ito M, Okamoto H, Nishioka S, Iijima K, et al. Modeling the detection efficiency of an HP-Ge detector for use in boron neutron capture therapy. Appl. Radiat. Isot. 2017;125:80–5.
[36] International Commission on Radiation Units and Measurements. Nuclear Data for Neutron and Proton Radiotherapy and for Radiation Protection (Report63).
[37] Beckurts KH, Wirtz K. Neutron Physics. Springer; 1964.

[38] Sato T, Iwamoto Y, Hashimoto S, Ogawa T, Furuta T, Abe S, et al. Features of particle and heavy ion transport code system (PHITS) version 3.02. J. Sci Nucl. Technol. 2018;55:684–90.
[39] Goorley T, James M, Booth T, Brown F, Bull J, Cox LJ, et al. Initial MCNP6 Release Overview. Nucl. Technol. 2012;180:298–315.
[40] Memarinan N, Rozati SM, Concinal I, Vomiero A. Deposition of nanostructured CdS thin films by thermal evaporation method: effect of subsrate temperature. Materials (Basel) 2017:10(7).
[41] Kisss AZ, Koltay E, Nyako B, Somorjai E, Anttila A, Raisanen J. Measurements of relative thick target yields for pige analysis on light elements in the proton energy interval 2.4-4.2 MeV. J. Radioanal Nucl. Chem. 1985;89:123–41.
[42] Radiation Shielding Information Center Data Library DLC-136/PHOTOX, National Institute of Standards and Technology.
[43] Minsky DM, Kreiner AJ, Valda AA. AB-BNCT beam shaping assembly based on ^{7}Li (p, n)^{7}Be reaction optimization. Appl. Radiat. Isot. 2011;69(12):1668–71.